Microsolvation of LiH^+ in Helium Clusters: Many-Body Effects and Additivity Models for the Interaction Forces

Enrico Bodo, Francesco Sebastianelli, and Franco A. Gianturco*

Department of Chemistry and INFM, University of Rome La "Sapienza", Piazzale A. Moro 5, 00185 Rome, Italy

I. Pino

Department of Physical Chemistry and Electrochemistry, University of Milan, via Golgi 19, Milan, Italy

Received: November 12, 2004; In Final Form: April 4, 2005

The ab initio calculation of the interaction forces between the LiH^+ molecular ion, at its equilibrium geometry, and several He atoms is carried out in order to isolate and assess the importance of many-body contributions in the search for realistic energy and geometry data. The full potential energy surface (PES) with a single helium partner is obtained first by using an aug-cc-pVQZ basis set for He and higher quality ones for Li and H. The calculations were performed at the CAS−SCF plus MRCI level for the lowest potential energy surface over a total of 480 grid points of the two intermolecular Jacobi coordinates, whereas the excited state surface has also been examined in order to exclude the presence of any significant nonadiabatic interaction between the two PESs. A numerical fit of the lower surface is presented and the general physical changes of the ionic interaction when going from the lower to the upper of the two potentials are described and discussed. The fairly limited importance of many-body effects for such systems is seen from further ab initio calculations including several He atoms: our results suggest that, at least in the present case, no strong charge migration occurs after He attachment, and therefore, one could realistically model larger clusters by implementing a sum-of-potentials approach via the presently computed PES.

I. Introduction

The study of the interactions in weakly bound systems has received a great deal of attention in the past few years because of the broad variety of subjects in which they play an increasingly more appreciated role and because of the correspondingly broad range of experiments that have provided intriguing evidence for such a role.[1−4] Furthermore, the possibility that one can glean meaningful information on the structural properties of weakly bound clusters formed by a large number of rare gases (which include atomic or molecular dopants) by constructing their multidimensional potential energy surfaces (PESs) as simple sums of two-body interactions[5,6] has also encouraged theoreticians to focus on some of the simpler systems for which experiments are available (or possible) and for which the ab initio calculations can provide accurate results, in turn successfully employed to analyze and understand experimental findings.[7]

Electronic excitations can additionally offer a useful method to probe the embedded dopants and to study their interactions which the special quantum solvent provided by a liquid helium environment or by a smaller helium droplet.[8] The possible, final presence of ionized species after the excitation, i.e., of a molecular ion, strongly deforms the "soft" liquid helium that is very sensitive to its interaction with the dopant and therefore produces dramatic changes on the equilibrium configurations of the quantum solvation shells. For example, the shell of He atoms surrounding an ion gets to be strongly compressed with respect to the corresponding neutral dopant because of "electrostriction" effects: the rigid shell containing about 30−50 He atoms around an ion has a diameter of only about 12 Å and is usually referred to as a "snowball".[2−10] This is to be compared with the corresponding formation of a "bubble" of about 34 Å in diameter[11] in the case of a free electron in liquid helium, where the Pauli exchange repulsion with the bound electrons of the surrounding atoms plays a significant role. The corresponding neutral dopants are therefore expected to lie in structural situations which are between the two extreme cases of the "snowball" and the "bubble" arrangements.

One interesting case in point is the LiH molecular ion, LiH^+, where the stronger ionic forces occur in conjunction with the particular electronic structure of this alkali hydride doublet state, where the extra electron is expected to somewhat counteract the electrostriction effects discussed above. The corresponding neutral system, in fact, exhibits very weak interactions with the helium atoms of a droplet and tends to be somewhat ejected from the center of the latter.[12,13]

One commonly used approach for the treatment of these systems made of rare gas (Rg) atoms and an atomic or molecular impurity is to assume that the total interaction can be calculated as the sum of pairwise potentials. Although this assumption is largely valid for the pure Rg cluster, it may be incorrect when an impurity is present. When the impurity is charged, it induces multipoles on the Rg atoms that in turn interact with each other giving rise to a repulsive nonadditive 3-body contribution to the total potential field. This contribution has been studied in detail for anionic impurities in Ar cluster[14] and turns out to be of the order of about of a few percent of the total interaction.

* Corresponding author. Fax: +39-06-49913305. E-mail: fa.gianturco@caspur.it.

10.1021/jp0448144 CCC: $30.25
Published on Web 04/22/2005

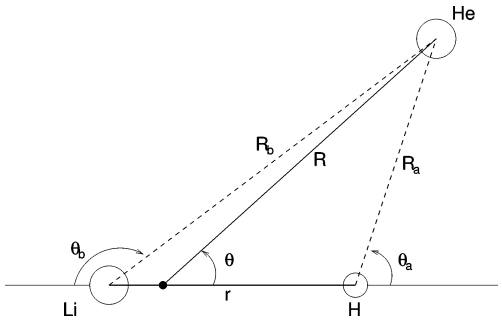

Figure 1. Intermolecular coordinates employed in the present study. The distance R is taken from the center of mass of LiH^+, for which the bond distance is fixed at 4.142 a_0. The labeled coordinates refer to those employed in the numerical fitting of the $X\ ^2A'$ surface (see section V for details).

TABLE 1: Basis Set for H Employed in the Present Calculations

type	exponent	coefficient	type	exponent	coefficient
s	837.22	0.000112	p	5.4	1.0
	123.524	0.000895	p	1.84	1.0
	27.7042	0.004737	p	0.57	1.0
	7.82599	0.0195518	p	0.28	1.0
	2.56504	0.065862	p	0.138046	1.0
	0.938258	0.178008	p	0.02	1.0
s	1.2	1.0			
s	0.36	1.0	d	0.3	1.0
s	0.15	1.0	d	2.13	1.0
s	0.07	1.0	d	0.67	1.0
s	0.04	1.0			
s	0.02	1.0	f	1.5	1.0
s	0.01	1.0			

It therefore does not alter substantially the structure and the energetics of the cluster (although it has more marked effect on electron affinities). Accurate numerical tests on Ne_nH^{-15} and $Li^+(He)_n$[16] clusters carried out by us have further confirmed this point.

In the present analysis, we therefore intend to discuss new computational results which describe the interaction of the LiH^+ molecular system, kept at the equilibrium geometry of its ground state, with one He atom. The electronic state considered in the main is the lowest one and the geometry mapped by the calculations evolve along the two-dimensional space of the Jacobi variables depicted in Figure 1: the (R,ϑ) coordinates. We have also computed the first excited state at the same molecular geometries in order to get some additional data on the charge-transfer features occurring upon excitation.

The following section briefly outlines our computational method and the main features of the interaction potential. Section III presents a numerical fitting of the present PES. Section IV, finally, looks at the features of the interaction forces in the smaller $LiH^+(He)_n$ clusters.

II. Interaction with a Single He Atom

A. Computational Details. The calculations were carried out using the GAMESS package,[17] with which we have computed the ground (X^2A') and first excited ($2^2A'$) electronic states of the $(LiHHe)^+$ system using a CAS−SCF molecular orbital optimization followed by an MR−CI expansion. The atomic basis set for Li was that optimized in ref 18, whereas the one for H was that optimized in our earlier work[19] and is reported in Table 1. The atomic basis set for He was the aug-cc-pVQZ standard expansion.[17] MRCI wave functions use single and double excitations out of a CAS reference space which includes 4 active orbitals and 5 active electrons. The molecular orbitals have been optimized at the 5-electron-in-6-orbital CASSCF level. Using larger active spaces in the CAS calculations did not change substantially the interaction energy of the ground state. This can be seen by the values reported in Table 2.

TABLE 2: Energies for the Ground State of the Present System Using Different CAS Active Spaces (Calculations for $\theta = 180''°$)

	$E(R = 4.0)$ a.u.	$E(R = 200.0)$ a.u.	difference (cm^{-1})
CAS(6)	−10.685142413	-10.682368027	−608.907
CAS(9)	−10.685137333	−10.682366654	−608.094

We computed a total set of 480 points given by 15 different ϑ values and 32 R values for each of them. The ground electronic state, with the LiH bond kept fixed at its optimum value of 4.142 a_0 (found by us with the same basis set of above for the isolated molecule and using the CAS−SCF plus MRCI procedure) exhibits its global energy minimum in the collinear configuration with $\vartheta = 180°$ and an R value of 4.125 a_0.

The charge behavior (at the ROHF level) is pictorially described by the results reported in Figure 2, where we show the changes undergone by the Mulliken and Lowdin charges on the three partner atoms, along the two opposite collinear orientations, as a function of the distance R. We see there that for distances beyond $R \sim 6\ a_0$ about 94.5% of the positive charge is localized on the lithium atom, 5.5% on the H atom while less than 10^{-6}% of the residual charge sits on the He atom, this being so along both collinear orientations: the system, as expected, is obviously dissociating as $Li^+H(X^2\Sigma^+) + He(^1S)$. A quick comparison of the lowest ionization potentials for the three partner atoms immediately confirms the energetic preference for an ionic lithium partner: $I_p(Li) = 520.2$ kJ/mol, $I_p(H) = 1312$ kJ/mol, $I_p(He) = 2372.3$ kJ/mol. We also see that on the collinear approach from the H-side of the molecular ion ($\vartheta = 0°$) the hydrogen acquires a negative charge while the helium atom becomes positively charged. This could be attributed to a sort of "through bond" electron density migration toward the lithium cation from the helium atom, ending, in part, onto the outer Li(2p) orbital. In the region where this happens, the potential, however, remains almost completely screened by the large Coulomb cusp due to the proximity of H and He. We therefore do not show in Figure 2 the region with $R < 4.0$ au for small θ. In that region, in fact, the charge distribution differs significantly from what we see in the outer region of the PES, and this is due to the incipient reaction that can lead to the formation of Li^+-He+H or to $Li+He-H^+$. This behavior suggest that it might be useful to also to look at the excited-state energies in order to exclude the presence of any interaction of the ground state with the excited one where the charge is localized on the H atom.

As a comparison between the two electronic states which we have obtained here, we report their total energy as a function of the internuclear distance for the collinear configuration ($\vartheta = 180°$) in Figure 3 for a limited range of distances: the actual calculations were carried out up to $R \sim 200a_0$.

One sees from that figure that the two PES differ asymptotically by 9.78 eV. However, from a separate study of the two electronic states of isolated LiH^+, we already know that the difference should correspond to $\Delta E \sim E_p(Li) - E_p(H)$ since the upper state exhibits the positive charge on the hydrogen atom.[23] The above value is 8.22 eV. The difference of 1.57 eV (0.0577 hartrees) can be attributed to the fact that, in our calculations, the equilibrium geometry of the molecular partner is the same in both states while the equilibrium distance of LiH^+ moves from 4.142 a_0 in the ground state to 7.43 a_0 in the $2^2\Sigma^+$ state.[23,24] Hence, in the present analysis, the second electronic

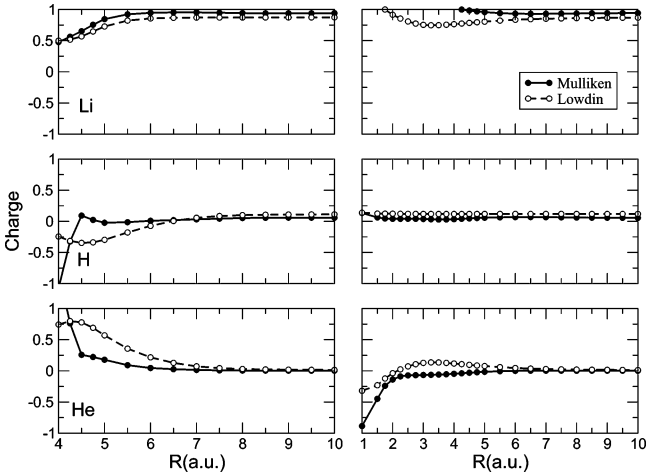

Figure 2. Computed Mulliken and Lowdin charges for the ground electronic state of $(HeLiH)^+$ as a function of the helium atom distance from the center of mass of LiH^+.

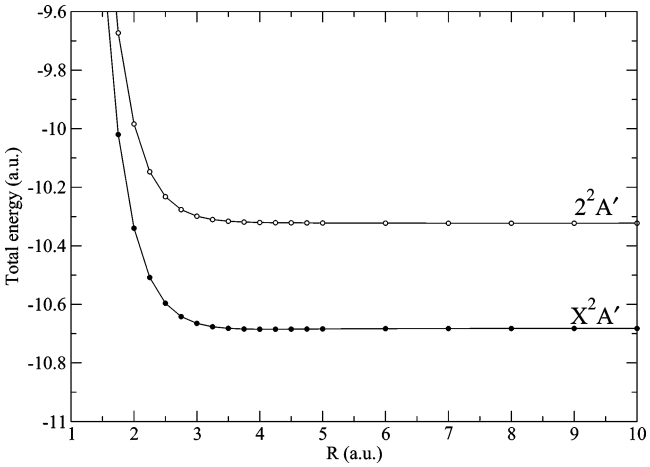

Figure 3. Computed CAS−SCF MRCI total energies for the lowest two electronic states of the $(LiHHe)^+$ system as a function of the radial coordinate.

state molecular geometry corresponds to an $LiH^+(2^2\Sigma^+)$ highly excited above its dissociation limit, where the above energy difference is being stored into "bond compression energy". Fuller calculations of the two PES with the additional variation of the LiH^+ bond are currently in preparation by our group and will be presented elsewhere.

B. Interaction Energy and Orientational Anisotropy. As it is well-known, the MRCI method is size-inconsistent so that, to obtain the interaction energy, one has to use either a correction for size consistency or to subtract asymptotes that have been calculated within the full system (i.e., LiH^+ and He separated by very large distances). Fortunately, in ionic systems, a third possibility that we deem to be the most accurate can also be used: the long-range potential for this system is given to a very good accuracy by the familiar form $V_{LR} = -\alpha_{He}/2R$.[4] We have simply shifted the computed points in order to match them with the long-range potential generated using the value of $\alpha_{He} = 1.34\ a_0$. Since the long-range potential is isotropic, the same asymptote has been used for all angles. The collinear potential curve thus reaches its minimum of $-619.7\ cm^{-1}$ at the radial value of $4.12\ a_0$ (the Li^+-He distance is therefore of about 3.6 au). It is interesting to notice how similar this value is to the one determined for the simpler Li^+He system.[20] The D_e in the latter is about $620-650\ cm^{-1}$ and the Li^+-He distance of about 3.5−3.6 au.

TABLE 3: Interaction Energies for the Ground State of the Present System Using MP4[a]

R (a.u.)	*E*(corrected), cm^{-1}	*E*(interaction), cm^{-1}	error (%)
3.7751	−469.61	−477.81	1.7
4.0251	−606.27	−613.30	1.2
4.2751	−600.78	−606.68	1.0
4.5251	-538.18	−543.11	0.9
4.7751	−459.53	−463.63	0.9
5.0251	−383.17	−386.62	0.9
5.2751	−316.10	−319.03	0.9
5.5251	−260.00	−262.49	1.0
5.7752	−214.17	−216.34	1.0
6.02521	−177.21	−179.11	1.0

[a] Second column: BSSE corrected values; third column: interaction energies obtained by subtracting the isolated monomers. The calculation is reported for various *R* and $\theta = 180"°$.

A second possible source of inaccuracy in the present calculation may be due to the lack of a proper correction for basis set superposition Error (BSSE). The Boys and Bernardi correction procedure[21] cannot be applied directly to the present calculations because it is size-inconsistent. However, to test the quality of our PES, we have performed an additional calculation with the same basis-sets using the size consistent MP4(SDQT) method as implemented in Gaussian 98.[22] The results obtained after correcting for BSSE the MP4 calculations and the interaction energies calculated by subtracting the two isolated fragments are reported in Table 3 together with their relative error. As one can see, the error in the well region is less than 2% of the total interaction, and therefore, we can safely assume that the BSSE error in our calculation is very small at least with respect to the interaction energies at play in the present system.

For the study of the microsolvating structures of the ionic impurity within the helium droplet or liquid, it is obviously important to be able to know the orientational anisotropy of the dopant interaction with each adatom in the solvating medium. This interest is based on the reasonable assumption (already discussed above) that in doped helium droplets the total interaction can be expressed as a sum of pairwise potentials. In the set of panels given by Figure 4, we therefore present the angular behavior of the interaction for the lowest electronic state $X\ ^2A'$. One clearly sees there that the angular region around $\vartheta = 0°$ (i.e., for the He partner approaching the H-atom side) the interaction remains largely repulsive, due to a strong nuclear repulsion cusp located around $3.6\ a_0$. It is only for angular values larger than 45° that the interaction resumes being more attractive: we therefore have an angular cone for the helium approach ($0° \le \vartheta \le 45°$) where the latter remains largely outside the molecular volume, with *R* beyond about $6\ a_0$, a feature that will be of in interest for the cluster studies that we shall later pursue with the present potential energy surface (PES). For larger angular values, on the other hand, we see that the helium interaction with the molecular ion (Li^+H) shows deeper minima, thereby generating potential wells which reach a minimum value of $-619.7\ cm^{-1}$ for the collinear configuration $He-Li^+-H$. This is essentially the most stable configuration for the complex.

The minimum region of the interaction energy, for three values of the θ angle, is presented in Figure 5 for better clarity. In the same figure, the computed points at the MP4 level (BSSE corrected and size consistent) are also reported as black circles in order to show the accuracy of the MRCI results.

C. Minimum Energy Configurations. When searching for the most stable quantum structures and for the ground-state wave functions of the helium clusters/droplets containing a molecular dopant,[3] it is of interest to know at best the spatial features of

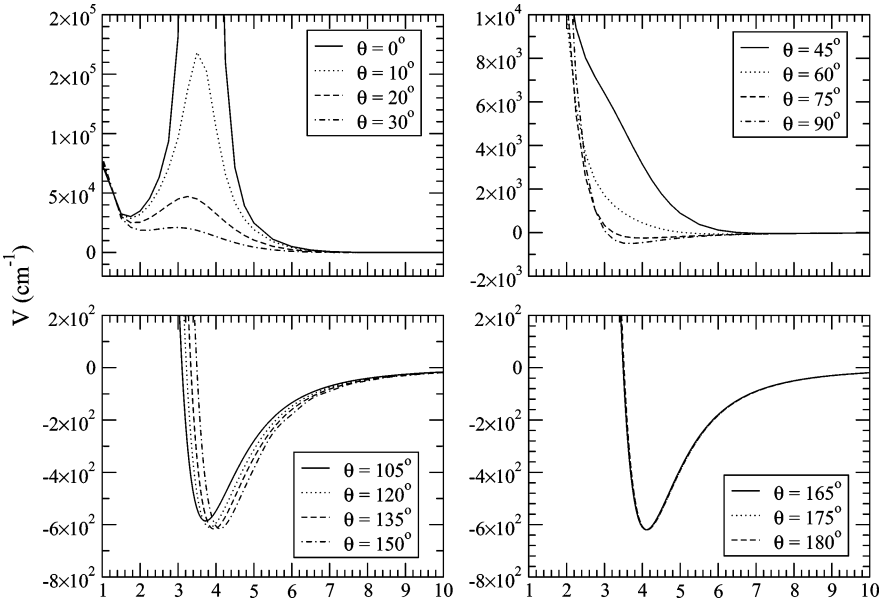

Figure 4. Computed interaction between the helium partner and LiH^+ in its ground electronic state The Jacobi coordinates are those defined in Figure 1. Distance in a.u.

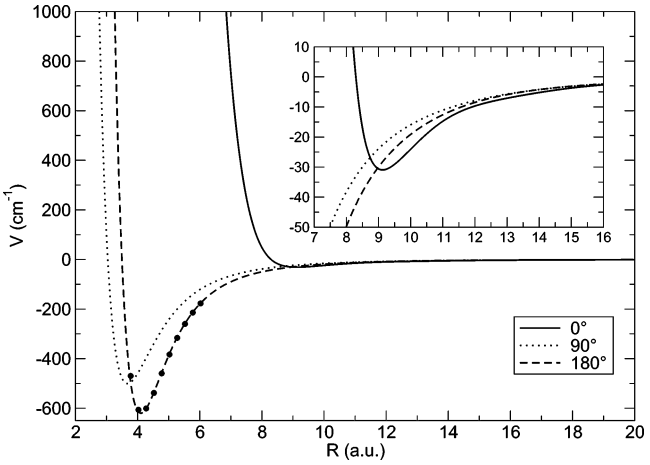

Figure 5. Computed interaction as a function of the radial coordinate and for three different ϑ. Black circles are the MP4 results reported in Table 3.

the overall interaction and to be able to locate the most likely configurations of the solvating atoms surrounding (or ejecting) the molecular impurity. We therefore present in Figure 6 the energy values of such minimum energy positions for the two PESs and in Figure 7 the corresponding radial locations of the same points.

The data related to the ground electronic state (lower panel) clearly show that the attractive well moves away from the center of mass when ϑ is small, i.e., for the He approaching the H-end of the target. On the other hand, we see from Figure 7 that increasing the value of ϑ brings the minimum of the attractive well much closer to the molecule (i.e., closer to its Li-end) and makes the interaction much stronger, down to its largest minimum value for the nearly collinear configurations. In fact, we see in that figure the spatial locations of the energy minima for the helium atom approaching the $(LiH)^+$ molecular target: The filled-in circles provide the data for the ground electronic state where the He partner gets much closer to the molecule once it locates itself on the lithium side of the target: the largest angle beyond which the helium atom starts to move out is about 90°, and it is indicated by an arrow in the map of minima locations.

The first excited state, on the other hand, shows its strongest attractive wells in the small angle region: the closest positioning of the He atom surrounding the ionic molecular target occurs now on the hydrogen side of the ion, where nearly all of the positive charge is located. Furthermore, the interaction energy is here much stronger (of the order of $\sim 10^4$ cm^{-1} and due to the formation of the stable molecular species HeH^+) and reaches its largest value for $\vartheta \sim 20°$, as marked by an arrow in the lower panel of Figure 7.

III. Numerical Fitting of the X $^2A'$ Surface

To employ the computed PESs for the structure of quantum solvents such as ^4He containing an ionic dopant,[8] it is certainly more expedient to be able to generate each interaction potential in some analytic fashion to improve on computational speed and efficiency. In the case of the ground-state PES discussed in the present work, the task is not trivial because of the marked orientational anisotropy of the PESs, further entangled with its strong radial dependence (e.g., see Figures 6 and 8). This means that it becomes difficult to perform up to convergence the conventional multipolar expansion

$$V(r_{eq}, R, \vartheta) = \sum_{\lambda} V_{\lambda}(R|r_{eq}) P_{\lambda}(\hat{R}\cdot\hat{r}) \qquad (1)$$

Following a similar strategy suggested earlier in ref 26, we therefore choose a different set of relative coordinates with which we shall describe the highly anisotropic region of the ground-state PES. These alternative coordinates are given in Figure 1 and are labeled by the two "atomic" indexes a and b for both the radial and angular variables.

The full interaction could then be written as

$$V_{tot} = V(R_a,\theta_a) + V(R_b,\theta_b) + V_{LR}(R,\theta) \qquad (2)$$

where each of the contributing terms is written down as

$$V(R_a,\theta_a) = \sum_{n=0}^{10}\sum_{l=0}^{2} R_a^n \exp(-\beta R_a)\, P_l(\cos\vartheta_a) C_{nl}^a \qquad (3)$$

and $V(R_b,\theta_b)$ is written in the same way. The long-range

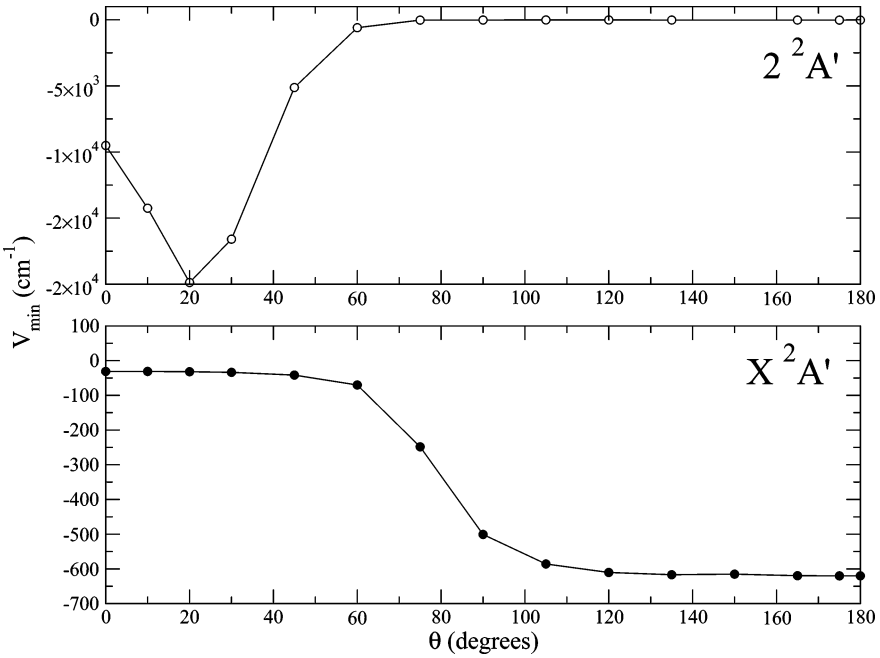

Figure 6. Computed minimum values of the interaction energies, for the two potentials discussed in the present work, given as a function of the Jacobi angle ϑ. The corresponding radial values could be qualitatively gleaned from Figure 7. Lower panel: ground electronic state. Upper panel: excited electronic state.

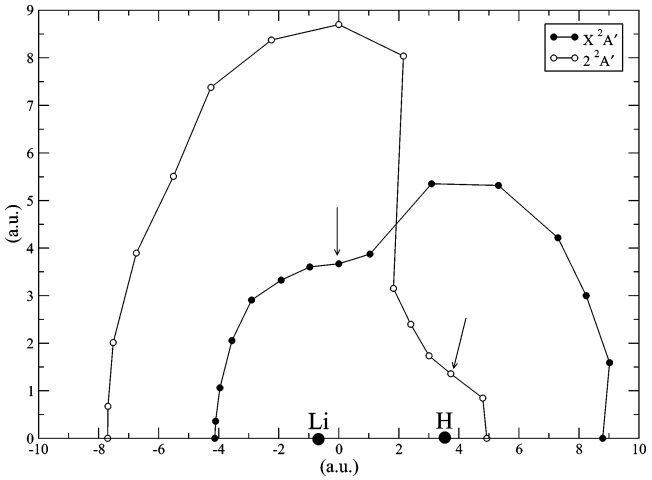

Figure 7. Positions of the minimum interaction energy for the He atom surrounding the $(LiH)^+$ target. The filled-in circles refer to the ground electronic state, whereas the open circles describe the first excited PES. The data are shown in cylindrical coordinates.

contribution is further given by

$$V_{LR}(R,\theta) = \sum_{n=4}\sum_{l=0}^{n-4} \frac{f_n(\beta R)}{R^n} P_l(\cos\vartheta) C_{nl}^{LR} \qquad (4)$$

where the f_n damping functions are those defined within the well-known Tang−Toennies empirical potential modeling.[27]

Because our chief interest lies in the study of low-energy processes, we have excluded some of the original raw points which correspond to the most repulsive regions of the interaction, at energy values well above those expected to be reached during subthermal dynamical processes. Thus, we performed the numerical fittings of 420 of the original 480 raw points mentioned earlier. The final accuracy of the fitting resulted in being of the order of 0.16 cm^{-1}. The final number of linear parameters needed for the fitting was 70 plus 1 nonlinear parameter β, involving the C_{nl}^{a}, C_{nl}^{b}, and C_{nl}^{LR} coefficients of eq 4. They are all available on request from the authors as well as the Fortran subroutine necessary to evaluate the PES. To give a better idea on the spatial shape of the PES, we report in Figure 8 a two-dimensional representation of it in terms of energy level values within an (x,y) representation of the Jacobi coordinates.

The figure clearly shows the strongly repulsive Coulomb cusps which surround the H atom and the largely attractive interaction region around the lithium atom, where nearly all the positive charge resides.

IV. Interaction Forces in $LiH^+(He)_n$

A. LiH^+He_2 System. As mentioned in the foregoing discussion, one of the aims of the present work is also that of assessing the quantitative importance of many-body (MB) effects on setting up the overall interaction for systems containing more than one He atom bound to the LiH^+ ionic impurity. The smallest unit in such a study is therefore given by the LiH^+-$(He)_2$ molecular complex. The MB contribution in this particular system arises from the mutual interaction between the various induced multipoles on the two helium atoms when they are in the presence of the ionic impurity. This is also the dominant contribution in larger clusters (e.g., see discussion in ref 14)

We first carried out a full geometry optimization of LiH^+-$(He)_2$ at the MP2 level (with all electrons included), employing for the lithium atom the cc-pVTZ basis set, while using the aug-cc-pVTZ for hydrogen and helium. We then performed a second MP2 optimization with quadruple zeta basis followed by a single-point MP4(SDQT) (with all active electrons) calculation. The resulting geometries and charges are reported in Table 4. The positive charge of the lithium atom has only partly moved onto the H atom and even less is being transferred onto the two helium atoms, which behave here as equivalent adatoms. The use of a larger basis set (cc-pVQZ for Li and aug-cc-pVQZ for He and H) and that of the MP4 level of calculation is seen to modify the charge situation only very little and further produces geometric changes which are noticeable but yet not very significant (less than 2%). The energy of LiH^+-$(He)_2$ is reported in the first row Table 5 together with the two

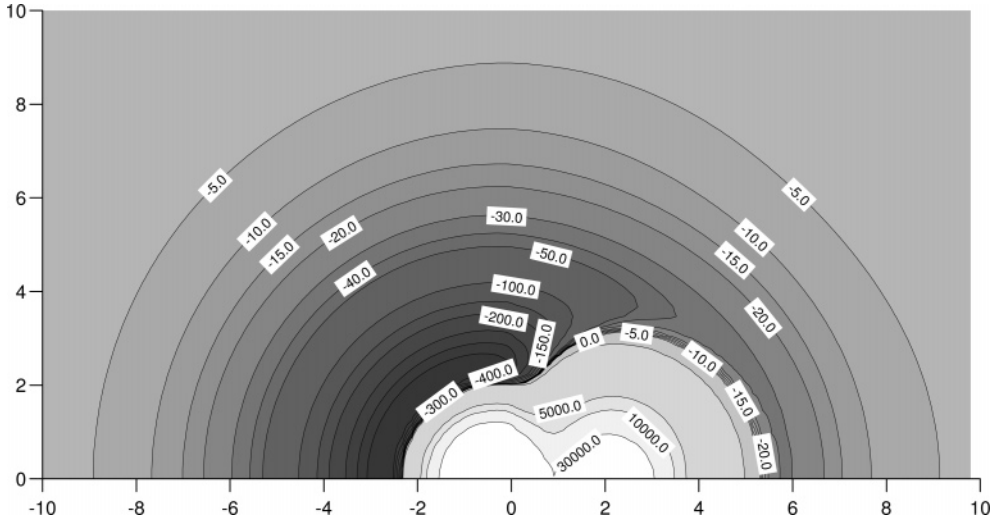

Figure 8. Energy level profiles in an (x,y) representation of the fitted PES for the ($X\ ^2A'$) electronic state. The Li is located at negative distance values. The energy profile are labeled in units of cm^{-1}. Distances are in Å.

TABLE 4: Optmized Geometries and Net Atomic Charges for the $LiH^+(He)_2$ System Carried out at Different Levels of Calculation[a]

property	MP2/(aug)-cc-pVTZ	MP4/(aug)-cc-pVQZ
R_{Li^+-H}	4.13	4.04
R_{Li^+-He}	3.54	3.51
R_{He-He}	5.55	5.55
charge (Li^+)	0.91	0.88
charge (H)	0.04	0.07
charge (He1)	0.02	0.02
charge (He2)	0.02	0.02

[a] Distance in a.u. See text for details charge resides.

fragments composing it in row 2 and 3. The energies have been calculated both for MP2 and MP4 with the triple and quadruple zeta basis, respectively, and applying the aforementioned BSSE correction.[21] Each of the fragment energies has been calculated by freezing it at the minimum geometry of the optimized LiH^+-$(He)_2$ complex.

We can easily obtain an estimate of the importance of the MB contribution to the total interaction energy by subtracting from the total energy of the $LiH^+(He)_2$ complex the various two-body contributions. Assuming that the three bodies at play in our system are the molecular impurity as a whole and the two helium atoms, we have three possible two-body contributions which are given by the energies of the two identical LiH^+−He structures and by the "compressed" He−He system (structures B and C in Table 5): for these three fragments, we have the three interaction energies labeled as A, B, and C in Table 5. The three-body contribution is simply given by the difference A-2·B−C which turns out to be 7.08 and 15.42 cm^{-1} respectively for MP2 and MP4. The three body contribution is repulsive because it arises mainly from the interaction between two induced dipole on the two helium atoms which are oriented in the same direction. This repulsive contribution is rather small when compared to the single binding energy of a helium atom to the LiH^+ molecule (i.e., energy B). It is important to point out however that this estimate relies on the rather crucial assumption that the molecular impurity behaves as a "single body". This is not entirely true since, for example, its internal distance varies, albeit by not much, when going from the LiH^+-He species to the $LiH^+(He)_2$ complex.

The two sets of calculations carried out at the MP2 and MP4 level of post-Hartree−Fock treatment of correlation effects indicate that there are fairly small quantitative differences between them but that both calculations provide very similar patterns of behavior for the energy balances involved in the "vertical" fragmentation processes. Additionally, the present calculations on the smallest complex formed by LiH^+ indicate that the MB effects are indeed present but are still rather small: "classical" estimates of the binding, in fact, show that the contributions are largely additive, that very little charge migrates from the ion onto the two helium atoms and that they remain essentially equivalent additions to the ionic core without signs of preferential binding or structuring of either of them to the LiH^+ dopant.

B. Smaller $LiH^+(He)_n$ Clusters. To further analyze the structural behavior of the clusters where more helium atoms are present, we carried out optimized geometry calculations of a few more $LiH^+(He)_n$ clusters, with n up to 7. The calculations were done using structures as a "classical" concepts, i.e., without the inclusion of zero-point energies (ZPEs). The various optimizations has been done with the MP2 method and the cc-pVTZ basis set. The corresponding spatial configurations are reported by Figure 9, where the various bond distances are also given. To all of the following structures, we did not apply any BSSE corrections.

The following comments can be readily made by examining the results of that figure:

1. If one remembers that the optimized structure of the LiH^+-He discussed in section 2 provided an ionic bond distance of 4.12 au, we see that the next two clusters leave that value essentially unchanged, whereas the larger clusters find an optimized ionic core structure with a stretched LiH bond: this is due to the increasing screening effects on the lithium positive charge induced by the larger number of helium atoms: in other words, this is an effect due to the MB interactions. The effect is certainly there, but it remains to be seen how much it may influence ZPE values given the possibly marked delocalization of the "solvent" helium atoms.

2. The fairly close equivalence of all of the helium atoms as their number goes up is also evident from the structural data of the smaller clusters up to $n = 5$ where all bond distances from the lithium atom remain very similar to each other.

3. For $LiH^+(He)_6$ and $LiH^+(He)_7$, we further see that the clusters still grow with equivalent He atoms being added to the ionic core and onto the Li^+ "side" of the molecule, but small differences begin to appear. One helium atom, in fact, remains on the molecular axis while a planar ring of further adatoms

TABLE 5: Computed Interaction Energies for the LiH^+He_2 Complex and for the Two Body Fragmentation Structures using the MP2/MP4 Method and Triple/Quadruple-ζ Basis Sets[a]

Fragment	Expression	Energy/MP2/TZ(cm^{-1})	Energy/MP4/QZ(cm^{-1})
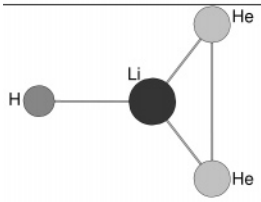	A) $E(LiH^+He_2) - E(LiH^+) - 2{\cdot}E(He)$	-1079.62	-1193.13
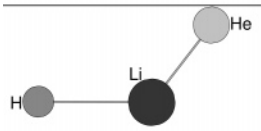	B) $E(LiH^+He - E(LiH^+) - E(He))$	-541.84	-601.25
	C) $E(He-He - 2E(He))$	-3.03	-6.05

[a] Interactions are calculated by using the counterpoise BSSE correction.

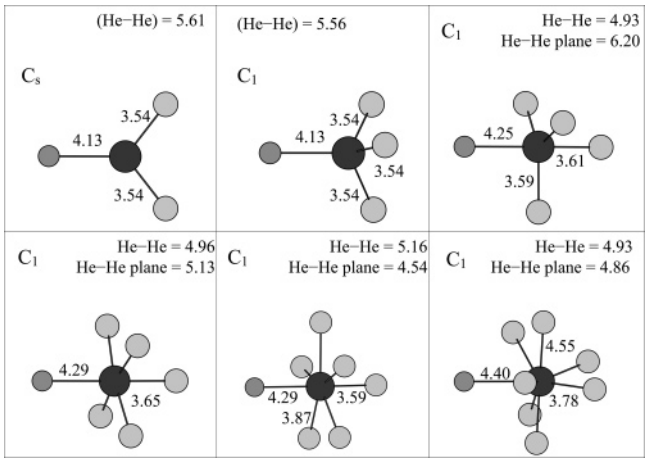

Figure 9. Computed ab initio configurations of the smaller $LiH^+(He)_n$ clusters with n from 2 to 7. The various panels show the Li atom (black), the H atom (gray), and the He atoms as lighter gray circles. Distances are all in a.u.

appears to surround Li^+ and to stabilize at slightly larger distances than that of the axial one.

One should remember, however, that we are discussing delocalized quantum systems for which the structural optimization is artificially carried out for classical structures where such delocalization disappears. It is interesting to see, however, that even such calculations (where MB effects are included) already show the structuring of the smallest clusters to be occurring with the adatoms energetically behaving as equivalent species that surround a nearly undistorted molecular ion.

The energetics of the present clusters is further presented by the data shown in Figure 10, where we report (on the upper panel) the single atom evaporative energy as a function of cluster size, whereas the lower panel shows the total binding energies of each of the clusters as n increases. The inset within that panel reports the binding energy per He atom along the same series of clusters.

The data on the evaporation energies, given by the upper panel of Figure 10, indicate (as expected) that the role of He−

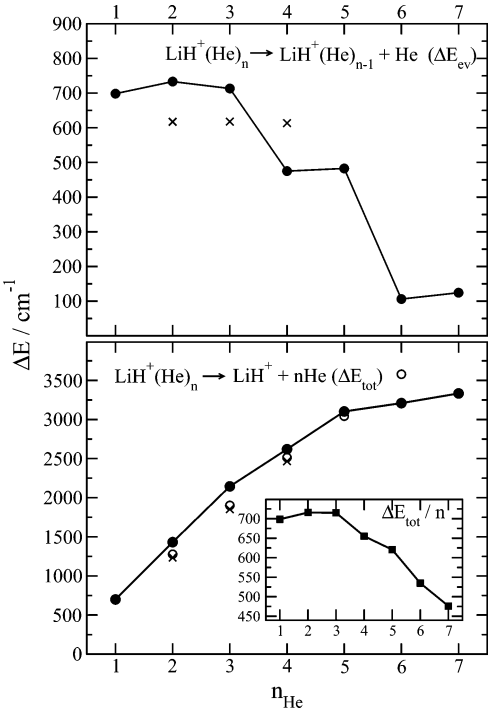

Figure 10. Computed energy differences along the clusters series of the present work. All values in cm^{-1}. Upper panel: single atom evaporative energies. Lower panel: total binding energies of the He atoms in each cluster. Inset within the lower panel: binding energy per He atom. The crosses are the same energies taken from ref 20, while the white circles in lower panel are from our work.[16] These two last set of data refer to purely atomic $Li^+(He)_n$ clusters.

He repulsions play an increasingly more important role as n gets larger. One further sees essential equivalence of the energy required to evaporate an He atom along the first three clusters, while a marked drop occurs for $n = 4$ and 6. Such reduced binding strengths could be explained, at least qualitatively, by the structures in Figure 9. We see there, in fact, that planar configurations for some of the helium atoms are formed and they increase their relative "crowding", shown by the reduction

of the He−He distances between the atoms on that plane. One extra atom remains out-of-plane, hence presumably more strongly bound to the ion. On the other hand, the effect of the latter is counterbalanced by the contribution of the other atoms, and the net effect is therefore one in which the binding per He atom gets reduced: the inset in the lower panel shows indeed that the average reduction occurs fairly smoothly for $n > 3$. Although the total binding energy increases as n increases, it indicates that already in the present small clusters such an increase reaches a sort of saturation. One expects, in fact, that in the larger clusters the screening of the charge at the molecular impurity becomes increasingly more efficient, thereby suggesting that the additional binding of more adatoms outside the core is largely driven by weaker induction forces and dispersion effects. Hence, each single adatom contribution to the total binding becomes increasingly more negligible with respect to the previous total value and should clearly show a saturation effect on the energetics of the curve given by the lower panel of Figure 10.

An interesting comparison can be made with the data for the similar although simpler cluster $Li^+(He)_n$. In refs 20 and 16, fully ab initio geometry optimization calculations were performed. The obtained energies, whenever available, are compared with the present ones in Figure 10. As one can see there, the energetics of the two kind of clusters is very similar. The reason is that in the molecular ion the charge is almost completely localized on the Li atom so that the He atoms tend to structure on its side where the interaction is the largest. Since, moreover, the Li^+−H molecule has a very large equilibrium distance, this "first shell" on the Li side is in a first approximation unaffected by to the presence of the H atom. This behavior is further confirmed by the fact that the geometries are also very similar: for the molecular cluster in the moiety with 4 helium, we find an Li^+−He distance of 3.54 au, whereas the same distance measures about 3.6 au in the case of an atomic Li^+ dopant.[20,16] However, one should expect that this simple behavior will be modified when the He atoms "crowding" around the Li side of the molecule will force the additional adatoms to move over onto the other side of the molecule. One still expects, however, that the H atom of the molecular ion will reduce the "electrostriction" effects on the solvent atoms with respect to the same effects for the purely atomic ion.

V. Conclusions

In the present work, we have analyzed first and in great detail the features of the interaction of the $(LiH)^+$ molecular ion with a single He atom in the case where the ionic target is kept at its equilibrium geometry. The calculations were carried out at the MRCI level using a fairly extended basis set, and we have probed the interaction forces by describing the potential field that surrounds the ionic impurity, estimating its orientational and spatial strength together with its overall anisotropic features.

The calculations found the ground electronic state PES to be very strongly anisotropic and to produce a minimum energy configuration that is nearly linear, with the He atom attached to the lithium side of the molecular ion. On the other hand, the first excited state showed very different behavior, with the charge of the ion residing nearly all on the H atom and with the He atom strongly bound to the latter, in a slightly off -linearity minimum energy configuration.

We have further analyzed the minimum energy structure of the next larger complex where the same ionic moiety is bound to two helium atoms. We found its "classical" structure to be of C_{2v} symmetry with the adatoms directly bound to the Li^+ side of the molecule. We further analyzed in that system the possible effect of many body interactions and found them to be indeed present but to be fairly small with respect to the main ionic forces that attach each of the He atoms to the Li^+ core. Such findings therefore suggest that one could possibly study larger clusters by using a sum-of-potentials approximation to the total intermolecular field. Within such scheme, then, the present fitting of the LiH^+−He PES could be profitably employed to describe the intra-cluster overall potential energy surface as given by

$$V(\mathbf{R}_{LiH^+},\mathbf{R}_{He}) = \sum_{k=1}^{k_{max}} V(\mathbf{R}_{LiH^+-He_k}) + \sum_{k,j} V(R_{He_k-He_j}) \quad (5)$$

Where $\mathbf{R}_{LiH^+}$ is the vector locating the center-of-mass of the molecular ion and $\mathbf{R}_{He}$ collectively represents all of the vectors locating the helium atoms. The "two-body" potentials on the rhs of eq 5 would therefore represent the sum-of-potential approximation, where the first summation collects separate replicas of our fit to the LiH^+−He PES and the second one includes some accurate description of the interactions between any pair of He atoms (see ref 27 for an example of it).

On the whole, the present calculations suggest, as expected, that the ionization of an LiH dopant within helium droplets, of within smaller He clusters, is likely to create a strongly bound molecular impurity that would be efficiently solvated within the quantum fluid. A study of the microsolvation process will therefore be the next step of our analysis and will be reported elsewhere.

Acknowledgment. The financial support of the Research Committee of Rome University, of the INFM, and of the CASPUR Consortium is gratefully acknowledged. We thank Dr. Martinazzo for useful suggestions in the preliminary stages of this work. We also acknowledge the support of the EU Training Network No. HPRN-CT-2002-00290 (Cold Molecules).

References and Notes

(1) See, for example: *Atomic and Molecular Beams, The state of the art*; Camargue, R., Ed.; Springer: Berlin, 2000.
(2) Gianturco, F. A.; Filippone, F. *Chem. Phys.* **1999**, *241*, 203.
(3) Toennies J. P.; Vilesov, A. F. *Annu. Rev. Phys. Chem.* **1998**, *49*, 1.
(4) *Advances in Atomic Physics*; Bederson, B., Walther H., Eds.; Academic Press: New York, 1997.
(5) Sebastianelli, F.; Di Paola, C.; Baccarelli, I.; Gianturco, F. A. *J. Chem. Phys.* **2003**, *119*, 5570.
(6) Sebastianelli, F.; Yurtsever, E.; Gianturco, F. A. *Chem. Phys.* **2003**, *290*, 279.
(7) Bodo, E.; Gianturco, F. A.; Yurtsever, E.; Yurtsever, M. *J. Chem. Phys.* **2004**, *120*, 9160.
(8) Stienkemeier, F.; Vilesov, A. F. *J. Chem. Phys.* **2001**, *115*, 10119.
(9) Padmore, T. C.; Cole, M. W. *Phys. Rev.* **1974**, *A9*, 802.
(10) Northby, J. *J. Chem. Phys.* **2001**, *115*, 10065.
(11) Jortner, J.; Kestner, N. R.; Rice, S. A.; Cohen, M. H. *J. Chem. Phys.* **1965**, *43*, 2614.
(12) Gianturco, F. A.; Bodo, E.; Martinazzo, R.; Raimondi, M. *Europhys. J.* **2001**, *D15*, 321.
(13) Taylor, B. R. private communication.
(14) Lenzer, T.; Yourshaw, I.; Furlanetto, M. R.; Pivonka, N. L.; Neumark, D. M. *J. Chem. Phys.* **2001**, *115*, 3578.
(15) Sebastianelli, F.; Di Paola, C.; Baccarelli, I.; Gianturco, F. A. *J. Chem. Phys.* **2003**, *119*, 5570.
(16) Sebastianelli, F.; Baccarelli, I.; Bodo, E.; Di Paola, C.; Gianturco, F. A.; Yurtsever, M. *Comput. Mater. Sci*. **2004**, in press.
(17) Schmidt, M. W.; Baldridge, K. K.; Boatz, J. A.; Elbert, S. T.; Gordon, M. S.; Jensen, J. H.; Koseki, S.; Matsunaga, N.; Nguyen, K. A.; Su, S. J.; Windus, T. L.; Dupuis, M.; Montgomery, J. A. *J. Comput. Chem.* **1993**, *14*, 1347.

(18) Yiannopoulou, A.; Jeung, G.; Park, S. J.; Lee, H. S.; Lee, Y. S. *Phys. Rev*. **1999**, *A59*, 1178.
(19) Martinazzo, R.; Tantardini, G. F.; Bodo, E.; Gianturco, F. A. *J. Chem. Phys*. **2003**, *119*, 11241.
(20) Sapse, A−M.; Dumitra, A.; Jain, D. C. *J. Cluster Sci*. **2003**, *14*, 21.
(21) Boys, S. F.; Bernardi, F. *Mol. Phys.* **1970**, *19*, 553.
(22) Frisch, M. J.; Trucks, G. W.; Schlegel, H. B.; Scuseria, G. E.; Robb, M. A.; Cheeseman, J. R.; Zakrzewski, V. G.; Montgomery, J. A., Jr.; Stratmann, R. E.; Burant, J. C.; Dapprich, S.; Millam, J. M.; Daniels, A. D.; Kudin, K. N.; Strain, M. C.; Farkas, O.; Tomasi, J.; Barone, V.; Cossi, M.; Cammi, R.; Mennucci, B.; Pomelli, C.; Adamo, C.; Clifford, S.; Ochterski, J.; Petersson, G. A.; Ayala, P. Y.; Cui, Q.; Morokuma, K.; Malick, D. K.; Rabuck, A. D.; Raghavachari, K.; Foresman, J. B.; Cioslowski, J.; Ortiz, J. V.; Stefanov, B. B.; Liu, G.; Liashenko, A.; Piskorz, P.; Komaromi, I.; Gomperts, R.; Martin, R. L.; Fox, D. J.; Keith, T.; Al-Laham, M. A.; Peng, C. Y.; Nanayakkara, A.; Gonzalez, C.; Challacombe, M.; Gill, P. M. W.; Johnson, B. G.; Chen, W.; Wong, M. W.; Andres, J. L.; Head-Gordon, M.; Replogle, E. S.; Pople, J. A. *Gaussian 98*, revision A.7; Gaussian, Inc.: Pittsburgh, PA, 1998.
(23) Gianturco, F. A.; Bodo, E.; Martinazzo, R.; Raimondi, M. *Chem. Phys*. **2001**, *271*, 032706.
(24) Gianturco, F. A.; Gori-Giorgi, P. *Astrophys. J*. **1997**, *479*, 560.
(25) Gianturco, F. A.; Gori-Giorgi, P.; Berriche, H.; Gadea, F. X. *Astron. Astrophys. Suppl. Ser*. **1996**, *117*, 377.
(26) Groenenboom, G. C.; Struniewicz, I. M. *J. Chem. Phys*. **2000**, *113*, 9562.
(27) Tang, K. T.; Toennies, J. P. *J. Chem. Phys*. **1984**, *80*, 3726.